### Title

Intramolecular signaling in a cardiac connexin: Role of cytoplasmic domain dimerization




### Authors

Trease, Andrew J
Capuccino, Juan MV
Contreras, Jorge
et al.



### Publication Date

2017-10-01

### DOI

10.1016/j.yjmcc.2017.07.010

Peer reviewed

HHS Public Access

Author manuscript

*J Mol Cell Cardiol*. Author manuscript; available in PMC 2018 October 01.

Published in final edited form as:

*J Mol Cell Cardiol*. 2017 October ; 111: 69–80. doi:10.1016/j.yjmcc.2017.07.010.

# Intramolecular signaling in a cardiac connexin: Role of cytoplasmic domain dimerization

**Andrew J. Trease**[1], **Juan M.V. Capuccino**[2], **Jorge E. Contreras**[2], **Andrew L. Harris**[2], and **Paul L. Sorgen**[1,*]

[1]From the Department of Biochemistry and Molecular Biology, University of Nebraska Medical Center, Omaha, NE 68198, USA

[2]Department of Pharmacology, Physiology and Neuroscience, New Jersey Medical School, Rutgers University, Newark, NJ 07103, USA

## Abstract

Gap junctions, composed of connexins, mediate electrical coupling and impulse propagation in the working myocardium. In the human heart, the spatio-temporal regulation and distinct functional properties of the three dominant connexins (Cx43, Cx45, and Cx40) suggests non-redundant physiological roles for each isoform. There are substantial differences in gating properties, expression, and trafficking among these isoforms, however, little is known about the determinants of these different phenotypes. To gain insight regarding these determinants, we focused on the carboxyl-terminal (CT) domain because of its importance in channel regulation and large degree of sequence divergence among connexin family members. Using *in vitro* biophysical experiments, we identified a structural feature unique to Cx45: high affinity ($K_D$ ~100 nM) dimerization between CT domains. In this study, we sought to determine if this dimerization occurs in cells and to identify the biological significance of the dimerization. Using a bimolecular fluorescence complementation assay, we demonstrate that the CT domains dimerize at the plasma membrane. By inhibiting CT dimerization with a mutant construct, we show that CT dimerization is necessary for proper Cx45 membrane localization, turnover, phosphorylation status, and binding to protein partners. Furthermore, CT dimerization is needed for normal intercellular communication and hemichannel activity. Altogether, our results demonstrate that CT dimerization is a structural feature important for correct Cx45 function. This study is significant because discovery of how

*To whom correspondence should be addressed: Department of Biochemistry and Molecular Biology, University of Nebraska Medical Center, Omaha, NE 68198., Phone: (402) 559-7557; Fax: (402) 559-6650; psorgen@unmc.edu.

**Disclosures**

The authors declare that they have no conflicts of interest with the contents of this article.

**Author contributions**

A.J.T. performed the experiments for Figures 1–7 and Supplemental Figure 1–3 as well as helped write the manuscript. J.M.V. performed the experiment for Figure 8. J.C. and A.L.H. coordinated the work performed by J.M.V., provided helpful discussion, and insightful comments throughout the study. P.L.S. conceived and coordinated the study and helped write the manuscript. All authors reviewed the results and approved the final version of the manuscript.

interactions mediated by the CT domains can be modulated would open the door to strategies to ameliorate the pathological effects of altered connexin regulation in the failing heart.

**Keywords**

Gap junctions; intercellular communication; Connexin45; carboxyl terminal domain; dimerization; protein-protein interactions

## 1. Introduction

Gap junctions are specialized membrane channels that connect the cytoplasms of adjacent cells. The direct cell-to-cell communication provided by gap junction channels is necessary for a number of physiological processes including signal propagation, organ tissue synchronization, and development [1]. Formation of intercellular channels occurs through the docking of connexons (hemichannels) from adjacent cells. Each connexon is comprised of six connexin proteins. Connexins, named for their molecular weights (e.g., 45 kDa isoform is connexin45; Cx45), are a family of 21 human isoforms that share a common topology: four transmembrane domains, two extracellular loops (EL), a cytoplasmic loop (CL), and cytoplasmic N- and C-terminal domains (NT and CT respectively). A high degree of sequence similarity exists within the transmembrane domains and the extracellular loops; the later contains six conserved cysteine residues vital to proper channel formation. The most divergent connexin domains are the CL and CT, with the CT playing a role in the trafficking, localization, and turnover of gap junction channels, as well as the level of intercellular communication via numerous post-translational modifications and protein-protein interactions [1, 2]. The CT is also important for regulating junctional conductance and voltage sensitivity [3–5]. This makes the CT a desirable target for isoform-specific pharmacological modulation of channel function [6–8].

Connexins are expressed in nearly all cell types and organ systems, and the distribution of family members is regulated spatio-temporally [9]. For example, connexin expression in the heart is dominated by Cx43, Cx40, and Cx45. Cx43 expression is ubiquitous, while normal Cx45 expression is primarily limited to cells of the specialized pacemaking and conductance system. Here, Cx45 voltage sensitivity plays a key role in the propagation of unidirectional current from the atria to the ventricles [10, 11]. Gap junctions in the ventricles are primarily composed of Cx43. However, Cx45 is upregulated in failing human hearts and is thought to be responsible for cell-to-cell coupling in Cx43-null ventricular myocytes [12–14]. Of note, recent evidence suggest ephaptic mechanisms might also account for residual conduction in Cx43 knockout mice [15, 16]. The resulting altered coupling and slowed conductance enhances susceptibility to ventricular tachy-arrhythmias [17]. Thus, while the contribution of Cx45 to intercellular current flow in the ventricular myocardium is thought to be minimal in healthy hearts, Cx45-mediated electrical coupling becomes dominant because of its pathophysiological overexpression in the failing heart. It is likely that even modest upregulation of Cx45 has a profound effect due to its ability to form heteromeric channels with the remaining Cx43 and have a dominant effect on the resulting gap junctions, thereby disrupt cardiac function in ways that even reduced levels (as much as 60%) of Cx43 could

otherwise maintain [17–23]). Unfortunately, little is known about the mechanisms that make each cardiac gap junction channel different, including the properties of Cx45 that make its up-regulation a potential arrhythmogenic substrate in the myocardium. Based upon these observations, we explored the possibility that intermolecular interactions involving the divergent CT of connexins affect gap junction regulation.

Previous work from our laboratory identified high affinity dimerization ($K_D$ ~100 nM) of soluble Cx45CT domains mediated by 6 hydrophobic residues aligned on one face of an α-helical region (A333-N361) [24, 25]. When each hydrophobic residue was replaced by glutamic acid (L335E, L338E, I324E, L349E, I353E, Y356E; construct named Cx45CT-6E; Fig. 1) dimerization was disrupted while the α-helical conformation was retained [24]. Based upon dimerization of cytosolic domains as a key regulatory mechanism of ion channels (e.g., IP3 receptor, [26]) and the role of connexin CT domains as important for proper channel function, mediated in part through protein partner interactions, here we set forth to determine the biological significance of Cx45CT dimerization in the function of Cx45.

## 2. Materials and Methods

### 2.1. Antibodies and detection reagents

α-Cx45-CT(MAB3101), α-mouse-HRP (H+L; 12-439), α-pS (05-1000), and α-Nedd4 (07-049) were purchased from EMD Millipore; α-Cx43 (C6219), α-β-catenin (C2206), and α-β-tubulin (T5201) were purchased from Sigma-Aldrich; α-E-cadherin-Alexa488 (#3195), α-HA-647 (#3444), α-Myc-555 (#3756), α-rabbit-Alexa555 (#4413), α-mouse-Alexa647 (#4410), Normal Rabbit IgG (#2729), and α-pY-1000 Multi-Mab (#8954) were purchased from Cell Signaling; α-mouse-Alexa488 (A-11001), Texas Red Dextran (10,000 Da; D1863), Lucifer yellow CH (L453), and Streptavidin-Alexa647 (S21374) were purchased from Life Technologies; α-rabbit-HRP (H+L; #20320) was purchased from Alpha Diagnostics; Neurobiotin (SP-1120) was purchased from Vector Labs; α-rabbit-HRP (Light chain; #211-032-171) was purchased from Jackson Immuno Research; α-Cx45-CL (ACC-207) was purchased from Alomone; Veriblot-HRP (ab131366) was purchased from Abcam; and DAPI (#02157574) was purchased from MP Biomedicals.

### 2.2. Alignments of the Cx45 dimerization domain

Clustal Omega [27] was used with default settings to align the region corresponding to A333-N361 of mCx45 with other available RefSeq orthologs. Species and respective accession numbers utilized were Mus musculus (gi|117712), Homo sapiens (gi|226693517), Rattus norviegus (gi|229485323), Gallus gallus (gi|117711), Canis lupis familiaris (gi|117710), Cricetulus griseus (gi|81864086), Mesocricetus auratus (gi|81863959), and Sus scrofa (gi|166220134).

### 2.3. *In cyto* dimerization assay

Madin-Darby canine kidney (MDCK) cells seeded on coverslips were transiently co-transfected with Lyn-HA-Cx45/6E-CT-mVenusN and Lyn-Myc-Cx45/6E-CT-mVenusC. Approximately 20 hrs after transfection the cells were rinsed 2x with 1x PBS and ice-cold

methanol fixed and immunostained as described below, and imaged. Plasma membrane measurements were made using the Zeiss profile measurement tool of at least 90 double-transfected cells for each condition at 630X and signal calculated as area under the curve. For ER/Golgi measurements images were exported to NIH ImageJ and ROIs were used to isolate the ER/Golgi and signal was measured as mean fluorescent intensity. Quantification of mVenus signal was normalized to Myc signal.

### 2.4. Molecular biology

Constructs for the *in cyto* dimerization assay were ordered as G-Block gene fragments (IDT) and were cloned into the pcDNA3.1+/Zeo vector (Invitrogen) by restriction digest and ligation. Cx45 WT was PCR amplified from a pGEM-HE (Clontech) plasmid containing the mouse sequence using primers to add overlap corresponding to the pD2529 vector (DNA2.0). Cx45 6E was obtained by PCR from a G-Block gene fragment using the same primers at Cx45 WT. The primer sequences were **5′-TCT AGA GCC GCC ACC ATG AGT TGG AGC TTC CTG-3′** and **5′-TTT TAG AGA CCT CAA CCT TAA ATC CAG ACG GAG GTC-3′**. Purified PCR products were assembled into the pD2529 vector using NEBuilder HIFI DNA Assembly Master Mix (NEB) per manufacturer protocol. Humanized Cx45 WT and 6E were obtained as G-block gene fragments and assembled into the pD2529 vector using NEBuilder per manufacturer protocol. To generate C-terminal eGFP fusions the eGFP cassette from p-eGFPN1 was PCR amplified and assembled into the pD2529 vector using the NEBuilder according to manufacturer protocol. The primers used in the PCR reactions were **5′- AGC TGT CTA GAG CCG CCA CCT GAA GAG CAG TGT CAG TCG ATC GCT GGC TCT TCA ATG GTG AGC AAG GGC GAG-3′** and **5′- CGC TTT TAG AGA CCT CAA CCT TAC TTG TAC AGC TCG TCC ATG-3′**. Mouse Cx45 WT and 6E were PCR amplified from the pD25529 vector and then assembled into the pD2529-eGFP vector by NEBuilder according to manufacturer protocol. The primers used for amplification of the mCx45 WT and 6E fragments were **5′- AGC TGT CTA GAG CCG CCA CCA TGA GTT GGA GCT TCC TG-3′** and **5′- TCC TCG CCC TTG CTC ACC ATA ATC CAG ACG GAG GTC TTC-3′**. All PCR amplifications were carried out using the Q5 High-fidelity master mix (NEB). Cloned plasmids were transformed into DH5α per standard protocol, cultured ON at 37°C on respective selective LB plates and mini-prepped with the GeneJet miniprep kit (Thermo) per manufacturer protocol. All constructs were sequenced by ACGT to ensure sequence accuracy.

### 2.5. Cell culture

MDCK cells (gift from Dr. Paul Lampe, Fred Hutchinson Cancer Center), HeLa cells (gift from Dr. Steve Caplan, University of Nebrasksa Medical Center) and Hek-293T cells (gift from Dr. Myron Toews, University of Nebraska Medical Center) were cultured in Dulbecco's modified Eagle medium (Corning) at 37°C in a humidified 5% $CO_2$ atmosphere. Medium was supplemented with 10% fetal bovine serum (Seradigm), 2 mM L-glutamine (HyClone), 1% pen-strep (Corning), and 0.2% Normocin (Invivogen). The selective agent puromycin (Tocris) was used, when appropriate, at empirically determined concentrations.

### 2.6. Transfections

**Transient:** MDCK at ~70% confluence were lipofected using the MDCK Avalanche (EZ Biosystems) reagent at 2.5:3.5 (plasmid:reagent) diluted in OptiMem under antibiotic free conditions. MDCK cells were analyzed ~20 hrs post-transfection. **siRNA:** MDCK clones stably expressing Cx45 WT or 6E at approximately 60% confluent were lipofected with stealth siRNA designed against endogenous canine Cx43 using Lipofectamine RNAiMAX according to manufacturer protocol under antibiotic free conditions, cells were cultured 48 hrs prior to any analysis. Complexes were generated in OptiMem. siRNA was designed using the Invitrogen design tool against the coding region (CDS) of accession number NM_001002951.3. siRNA duplex sequence: **5′-UAA CAC UCA ACA GCC UGG UUG UGA A-3′** and **5′-UUC ACA ACC AGG CUG UUG AGU GUU A-3.′**

### 2.7. Stable clone generation

Approximately 70% confluent MDCK and Hek-293T cells were lipofected with SalI linearized mCx45 WT, mCx45 6E, hCx45 WT (MDCK only), hCx45 6E (MDCK only) using either MDCK Avalanche (MDCK; 2.5:3.5) or Lipofectamine 2000 (Hek-293T; 1:1) in OptiMem. Transfections were carried out under antibiotic free conditions, and cells were cultured 48–72 hrs prior to addition of selection media. MDCK and Hek-293T were selected with 5 μg/mL and 2 μg/mL puromycin respectively. hCx45 WT, hCx45 6E, and Hek-293T cells were bulk selected while mCx45 WT and 6E as well as mCx45 WT-eGFP and 6E-eGFP expressing cells were clonally selected using Whatman paper cloning disks. Western blots and immunofluorescence were used to screen clones, the final clone for each mCx45 WT and 6E was selected based on greatest transgene and lowest endogenous Cx43 expression. Endogenous Cx43 expression was not assessed in eGFP fusion expressing clones.

### 2.8. Immunofluorescence

Cells seeded on glass coverslips were rinsed 2x with 1x PBS and then fixed and permeabilized with either ice cold methanol at −20°C for 15 min or buffered formalin (1x PBS, 3.7% formaldehyde, 0.3% Triton X-100) at 37°C for 30 min. Coverslips were washed 3× 5 min in 1x PBS with gentle agitation and then blocked for 60–90 min at 37°C (1x PBS containing 1% bovine serum albumin and .3% Triton X-100). Coverslips were then incubated with the indicated primary antibodies diluted in blocking buffer for either 1 hr at RT or overnight at 4°C. Coverslips were washed 3x with 1x PBS and then incubated with secondary antibody (if necessary) 1 hr at RT and then washed 1x for 5 min with 1x PBS containing 100 ng/mL DAPI and then 2x 5 minutes with 1x PBS. Coverslips were mounted on a drop of SlowFade anti-fade (Life Tech), sealed with clear nail polish, and imaged.

### 2.9. Confocal imaging

All still images acquired on a Zeiss 710 LSM Confocal system using appropriate excitation and appropriate filter sets.

### 2.10. Live imaging

Live imaging dishes (In Vitro Scientific) were coated with bovine plasma fibronectin (Sigma) at 10 μg/mL. MDCK clones expressing Cx45 WT-eGFP or 6E-eGFP were seeded and imaged at confluence. Images were acquired over a 1 hr period at 1 min intervals on a Zeiss 710 LSM confocal microscope with definite focus module.

### 2.11. Western blot

Cultured cells were rinsed 2x with 1x PBS and then incubated with protease inhibitor buffer (PIB; 1x PBS containing 1x Roche Complete + EDTA, 2 mM PMSF, 2 mM Pepstatin A) on ice for 20 min and then harvested with a cell scraper. Cell suspensions were pelleted at 1500 RPM for 5 min at 4°C. PIB was removed and cell pellet resuspended in an appropriate volume of lysis buffer (PIB + 1% Triton X-100, unless otherwise specified), mechanically lysed and incubated on ice for 30 min. Lysates were quantified by bicinchoninic acid assay (BCA; Pierce) and normalized with lysis buffer. 30 μg of total protein lysate (unless otherwise indicated) was resolved by SDS-PAGE, transferred to PVDF (EMD Millipore), blocked either 2 hr at RT or ON at 4°C with either 5% non-fat milk/PBST or 5% BSA/TBST and incubated with indicated primary antibody in blocking buffer either 1 hr at RT or ON at 4°C. Blots were washed 3x for 10 min with either PBST or TBST, and then incubated for 1 hr at RT with secondary antibody. Membranes were then washed 4x 10 min each with either PBST or TBST and detected using Signal West Femto kit (Thermo) per manufacturer protocol and exposed to autoradiography film. Quantifications were done using NIH ImageJ software using a minimum of three independent replicates.

### 2.12. RT-PCR

MDCK clones expressing mCx45 WT and 6E were seeded and cultured to confluence. Cells were rinsed 2x with 1x PBS and lysed for RNA content using the GeneJet RNA Isolation kit (Thermo) per manufacturer protocol. Equivalent masses of RNA were reverse transcribed using the MuMV-RT kit (NEB) per manufacturer protocol with OligoDT priming. Equal volumes of each RT reaction were used as template for standard PCR reactions with primers to mCx45-WT/6E (**5′- ACAGTAAAAGGAGGGAACTTGAT-3′** and **5′-TGGCTTTGTTTTGCTTGTAGG-3′**) and GAPDH (**5′-GTAGTGAAGCAGGCATCGGA-3′** and **5′- GTCGAAGGTGGAAGAGTGGG-3′**) using Taq Green Master Mix (Thermo). Cycling was carried out as follows: Initial denaturation 95°C for 2 min, followed by 30 cycles of 95°C denaturation for 30 sec, 54.5°C annealing for 30 sec, and 72°C extension for 30 sec, followed by final extension of 5 min at 72°C. Equal samples volumes were analyzed by 2% Agarose/TAE electrophoresis spiked with ethidium bromide. No reverse transcriptase reactions were used to subtract genomic background. Quantification was done using NIH ImageJ software, normalizing samples to GAPDH loading control. Quantification was done using 3 independent replicates.

### 2.13. Co-immunoprecipitation

MDCK cells stable expressing either Cx45 WT or 6E were seeded in either 10 or 15 cm plates and grown to confluence. Cells were rinsed 2x with 1x TBS + 1mM EDTA and then scraped up an either 0.5 or 1.0 mL of IP lysis buffer (25mM Tris, 150mM NaCl, 0.25%

sodium deoxycholate, 0.05% SDS, 1% TX-100 plus protease and phosphatase inhibitors). Cells were mechanically lysed and then incubated for 30 min at 4°C with rotation. Lysates were precleared with normal rabbit IgG (2 μg) bound protein G agarose for 1 hr at 4°C and then clarified by centrifugation. Clarified lysates were quantified by BCA (Pierce) and normalized. Input samples were reserved and either 2 or 5 mg of lysate was immunoprecipitated with either 2 or 3 μg of rabbit α-Cx45 (Alomone) ON at 4°C. Immune-protein complexes were captured by 2 hr 4°C incubation with protein G agarose (Pierce), washed 5x with IP wash buffer (IP lysis buffer excluding sodium deoxycholate). Immunoprecipitated proteins were eluted using 35–50 μL 3x SDS sample buffer. Equal volumes of each sample were analyzed by western blot and to avoid cross reactivity with the IP antibody a light chain specific secondary antibody (Jackson) or Veriblot (Abcam) were utilized for detection. Quantification was done using NIH ImageJ software from 3 independent replicates.

### 2.14. Detergent solubility assay

The Triton X-100 solubility assay was modified from a method described previously [28]. Briefly, MDCK cells grown in 10-cm Petri dishes were washed with PBS and incubated in 1 mL PIB for 20 min at 4°C, harvested in the same buffer and gently pelleted. Supernatant was aspirated and cell pellet resuspended in 1 mL of fresh PIB supplemented with 50 units of Benzonase and mechanically lysed. Lysates were quantified by BCA and normalized. A total of 450 μL of cell lysate was brought to 1% SDS with 10% SDS, and reserved as total lysate. Another 450 μL was brought to 1% Triton X-100 with 10% Triton X-100 in 1x PBS and incubated at 4°C for 30 min with agitation. The Triton X-100 lysate was then separated into non-junctional (supernatant; soluble) and junctional (pellet; insoluble) fractions by ultracentrifugation at 100,000 x g for 1 hr at 4°C. The supernatant was carefully removed and retained as the soluble fraction. The pellet was solubilized in 500 μL of solubilization buffer (1x PBS, 8 M urea, 2.5% SDS, 0.1 M DTT, 1x Roche complete + EDTA, 2 mM PMSF, and 2 μM Pepstatin A). Volume normalized samples of total lysate (T), Triton X-100 soluble (S) and Triton X-100 insoluble (I) portions were analyzed by western blot. Soluble and insoluble fractions were quantified as a function of total lysate. Quantification was done using NIH ImageJ software from 3 independent replicates.

### 2.15. *In situ* detergent extraction

The in situ detergent extraction was previously described by [29]. Briefly, MDCK cells were seeded on glass coverslips (Neuvitro) and cultured to ~90% confluence. Coverslips were rinsed 2x with 1x PBS and then incubated for 30 min at 4°C with gentle agitation with either mock extraction buffer (1x PBS containing 1x Roche complete + EDTA, 2 mM PMSF, and 2 μM Pepstatin A) or extraction buffer (mock buffer + 1% Triton X-100). Following extraction, the cells were fixed and immunostained and images acquired. Extractions were performed on 3 independent replicates to ensure reproducibility. Quantification of remaining immunostain was done by taking the DAPI normalized MFI of the Cx signal in extracted images as a percent of signal in the mock images using ImageJ.

### 2.16. Hemichannel function assay

To assess hemichannel activity we modified the protocol described by [30]. Briefly, all buffers were pre-warmed to 37°C prior to beginning the experiment. MDCK clones expressing either Cx45 WT or 6E were seeded on glass coverslips were cultured to approximately ~90% confluent. Some wells were pretreated with either 100 μM $La^{3+}$ (Sigma) or freshly prepared 100μM pervanadate or both for 15 min prior to $Ca^{2+}$ washout and dye uptake. The presence of $La^{3+}$ was maintained during dye uptake. Cells were rinsed 1x with HBSS +$Ca^{2+}$/$Mg^{2+}$ (Life Tech) and then 2x with HBSS –$Ca^{2+}$/$Mg^{2+}$ (Life Tech). Cells were then incubated at 37°C with HBSS – $Ca^{2+}$/$Mg^{2+}$ containing Neurobiotin (0.1 mg/mL; Vector labs) for 10 minutes. Cells were then washed 2x with HBSS +$Ca^{2+}$/$Mg^{2+}$ to close hemichannels and gap junctions. Cells were formalin fixed and stained with streptavidin 647 conjugate (Life Tech) and imaged. Control cells were treated identically except all incubations were done in HBSS +$Ca^{2+}$/$Mg^{2+}$. 3 independent replicates were used for quantification calculated by DAPI normalized mean fluorescent intensity in Zen Blue (2012) where 15 fields of view were acquired per replicate. Results presented as mean + s.e.m. of all replicates.

### 2.17. Dye-transfer assay

Cells were scrape loaded as previously described [31]. Briefly, all buffers were pre-warmed to 37°C prior to beginning the experiment. Stable expressing MDCK clones were seeded on bovine plasma fibronectin (Sigma; 10 μg/mL) coated 35 mm live imaging dishes (CellStar). MDCK cells were transfected with Cx43 siRNA with Lipofectamine RNAiMAX (Life Tech) according to manufacturer protocol and then cultured for 48 hrs prior to scrape loading. After transection cells were washed 1x with 1x PBS and then overlaid with dye tracer mix (1x PBS containing Lucifer yellow, Neurobiotin, and Texas Red Dextran). Scrapes were introduced using a fine edged micro-scalpel and incubated at RT for 1 min. Tracer dye was gently washed away with 1x PBS and media was added and the cells returned to the incubator to culture for 5 min to allow dye to transfer. Following the dye transfer period the cells were washed with 1x PBS containing 1 mM $CaCl_2$ and 1 mM $MgCl_2$ to stop dye spread. Coverslips were then formalin fixed and stained as described above and imaged. 15 consecutive fields of view were acquired per replicate.

### 2.18. Cycloheximide chase

MDCK clones expressing mCx45 WT or 6E were cultured to approximately 90% confluent. Cells were rinsed 2x with 1x PBS and the incubated with fresh medium containing 80 μg/mL cycloheximide (Cell Signaling) for the indicated time points. Following the desired incubation time, the cells media was spiked with 10x Roche Complete + EDTA and the cells were harvested and pelleted at 1500 RPM for 5 min at 4°C. The supernatant was removed and the cells were lysed directly in 1x sample buffer supplemented to 1x PBS, with protease inhibitors and 50 units Benzonase. Equal volumes of sample were resolved by SDS-PAGE and analyzed by Western blot. Each time point was normalized to loading control and then to the starting time point.

### 2.19. Channel expression and molecular biology

cDNAs for Cx45WT and 6E mutant were subcloned into the pGEM-HA vector (Promega) for expression in *Xenopus* oocytes. Vectors were linearized with Nhe1 and transcribed in vitro to cRNAs using the T7 or SP6 Message Machine kit (Ambion).

### 2.20. Electrophysiology

Electrophysiological data were collected using the two-electrode voltage clamp technique (TEVC). Recordings were made at room temperature (20–22°C). The recording solutions contained (in mM) 118 NaCl, 2 KCl, 1.8 mM $Ca^{+2}$, 5 HEPES (pH=7.4). Currents from oocytes were recorded 1–3 days after cRNA injection using an OC-725C oocyte clamp (Warner Instruments). Currents were sampled at 2 kHz and low pass filtered at 0.2 kHz. Microelectrode resistances were between 0.1 and 1.2 MΩ when filled with 3 M KCl. Recordings were performed using agar bridges connecting bath and ground chambers. Endogenous Cx38 expression was reduced by antisense oligonucleotide against Cx38 injected 4 hr after harvesting the oocytes. After 1 day, the same oocytes were coinjected with 18–50 nL of cRNA (0.5–1 mg/mL) for Cx45 WT or 6E, plus the Cx38 (1 mg/mL) antisense. Hemichannel currents were elicited by a set of depolarizing pulses from a holding potential of −80 mV to a range of potentials from −50 to +80 mV in 10mV steps.

## 3. Statistical Analysis

All data were analyzed by using GraphPad Prism 5.0 and were presented as the mean + s.e.m. Statistical analysis performed in GraphPad Prism 5.0 was either one-way ANOVA with a Neuman-Keuls post-hoc analysis or Student's T-Test where appropriate. *P*-values <. 05 were considered statistically significant.

## 4. Results

### 4.1. Cx45CT dimerization at the plasma membrane

Cx45CT dimerization was initially identified through the use of a recombinantly expressed soluble peptide *in vitro* [24]. We posited that regulatory and structural features of the isolated CT peptides would be recapitulated in cells. The first step was to determine whether the CT domains expressed at the plasma membrane would dimerize. To do so, we applied a bimolecular fluorescence complementation (BiFC) assay to the Cx45CT WT and 6E constructs. Design of the BiFC constructs is diagramed in Fig. 2A. A N-terminal Lyn kinase domain was chosen as the membrane anchor mediated by myristoylation and palmitoylation. HA or MYC tags were used to differentiate the N- or C-terminal mVenus fragments upon staining, respectively, as well as to quantify the level of protein expression. When the MDCK cells are transfected with both the N- and C-terminal mVenus fragments, the fluorescence signal should be detected only if two Cx45CT domains interact, thereby enabling the mVenus fragments to be close enough to properly refold. For both the Cx45CT WT and 6E constructs, mVenus signal was detected only in those MDCK cells expressing both the HA and MYC tagged constructs (Fig. 2B). The fluorescence signal at the plasma membrane was quantified from 90 WT and 92 6E cells (collected from three independent experiments). To control for potential differences in expression and trafficking to the plasma

membrane for the WT and 6E proteins, the mVenus signal was normalized to the Myc tag signal for each construct (Fig. 2B). The signal for the Cx45CT WT at the plasma membrane was approximately 2.5-fold greater than that for Cx45CT 6E. This suggests the CT domain of Cx45 dimerizes when tethered to the plasma membrane and that the dimerization can be substantially inhibited by 6E. mVenus signal for both the Cx45CT WT and 6E constructs was also observed in the endoplasmic reticulum/Golgi apparatus at similar levels (Fig. 2B). We suspect the reason why there is any mVenus signal at all in the plasma membrane and Golgi/ER in the 6E images is because of localized concentration, as the tendency for the mVenus to refold is a condition of proximity. Thus, proximity leads to “background” mVenus signals that does not necessarily arise from dimerization. Importantly, any reduction in the mVenus signal of 6E relative to WT, normalized to myc, is significant, indicating less dimerization. On a technical note, this assay was attempted with full length Cx45 WT and 6E, and we did not observe a significant difference in the mVenus signal at the plasma membrane. We speculate that formation of a connexon (i.e., six connexins) placed the CT domains in close enough proximity (like what was observed in the endoplasmic reticulum/Golgi apparatus) for the mVenus fragments to properly refold, regardless of the CT dimerization state or potential CT interaction with other cytoplasmic domains (data not shown).

### 4.2. Cx45CT dimerization affects Cx45 degradation

To characterize the functional significance of Cx45CT dimerization, stably expressing Cx45 WT and 6E clones in Cx43 deficient MDCK cells (generous gift from Dr. Paul Lampe) were generated. Western blots showed an increase of approximately 2.5 fold Cx45 6E expression relative to Cx45 WT (Fig. 3A; three replicate samples are presented). Interestingly, we see a shift in the apparent molecular mass of Cx45 6E compared to the WT; a result consistent with a study that examined the effects of proteins containing disproportionate numbers of acidic amino acids [32]. We also screened for Cx43 expression as its residual expression could confound results in subsequent studies due to presence of Cx43 homomeric or Cx43/Cx45 heteromeric channels. Surprisingly, Western blot showed that all clones expressing Cx45 WT, but not 6E, expressed a small amount of Cx43 (Fig. 3A). Therefore, experiments were performed with and without knockdown of Cx43 (siRNA against Cx43; Supplemental Figure 1A); no difference in the results (e.g., gap junction formation or localization) was observed between the groups.

RT-PCR was used to determine if the increased Cx45 6E protein was the result of increased synthesis at the transcript level. Interestingly, the mRNA expression for both Cx45 WT and 6E was identical (Fig. 3B). This suggests that the increase in 6E protein was not the result of increased synthesis but could be the result of decreased degradation. To test this possibility, we used a cycloheximide (CHX) chase assay, where CHX is used to inhibit protein synthesis. Each of the clones were cultured in the presence of 80 μM CHX for a period of 12 hrs. Over time Cx45 WT was degraded, resulting in an approximate reduction of total protein by >80%. Conversely, the Cx45 6E protein level remained largely unchanged over the same 12 hr period, suggesting that the 6E form can escape normal mechanism(s) of degradation (Fig. 3C).

### 4.3. Cx45CT dimerization affects Cx45 plasma membrane localization

Based upon the difference in expression level between Cx45 WT and 6E, immunofluorescence was used to determine the influence of CT dimerization on cellular localization. Similar to a published study, Cx45 WT in MDCK cells was found in a punctate pattern at the plasma membrane (Fig. 4A, left panels, red) [33]. On the other hand, more Cx45 6E protein was localized at the plasma membrane and in a linear pattern (Fig. 4A, right panels, red). Quantification of the length confirmed this difference between Cx45 WT and 6E at the plasma membrane (mWT, 602 ±141 nm, 113 plaques; m6E, 1330 ±343 nm, 208 plaques; significance, <0.0001). Importantly, knockdown of endogenous Cx43 did not alter Cx45 WT protein localization (Supplemental Fig. 1B). To ensure these phenotypes were not species or cell line specific, we also immunostained using an antibody to the human Cx45 sequence expressed in MDCK cells (Fig. 4B; WT, left panel, red; 6E, right panel, red; length, hWT 640 ±236 nm, 311 plaques; h6E 1756 ±340 nm, 131 plaques; significance, <0.0001) as well as the mouse Cx45 sequence expressed in Hek-293T cells (Fig. 4C; WT, left, red; 6E, right, red; length, mWT HEK 749 ±365 nm, 141 plaques; m6E 1325 ±776 nm, 137 plaques; significance, <0.0001). In both cases, a similar plasma membrane distribution was observed for both Cx45 WT and 6E as in Fig. 4A. Additionally, to ensure this phenotype was not the result of either antibody affinity or fixation artifacts, a C-terminal eGFP fusion of either Cx45 WT or 6E stably cloned into MDCK cells was used for live imaging. Consistent with all the other data, the eGFP fusion proteins mirrored the stained phenotype exactly, with comparable levels of Cx45 WT (Fig. 4D, left panel) and a disproportionally larger amount of Cx45 6E (Fig. 4D, right panel) diffuse across the majority of the plasma membrane (Fig. 4D, left panel). A cursory measurement of the length of the WT gap junctions in the eGFP fusion yields an average gap junction length of 667 ±240 nm for a total of 12 plaques, suggesting that eGFP fusions are not altering the length of WT junctions and therefore unlikely to result in the diffuse membrane signal observed for the 6E-eGFP.

### 4.4. CT dimerization is necessary for proper junctional plaque formation

The immunofluorescence and live imaging experiments demonstrated that inhibiting Cx45CT dimerization results in an increased amount of the protein at the plasma membrane. To test if Cx45 6E are in junctional plaques, we performed a Triton X-100 solubility assay to quantify the junctional (insoluble) and non-junctional pools (soluble). When compared to Cx45 WT, 6E had a statistically significant ~1.6 fold increase in the non-junctional pool, and a corresponding decrease in the junctional pool (Fig. 5A; knockdown of Cx43 did not alter Cx45 plaque formation, Supplemental Fig. 1C). *In situ* Triton X-100 extractions produced comparable results and quantification of the Cx45 immunofluorescence revealed approximately 40% of signal remains for WT yet the residual signal for 6E is approximately 18%, which correlates with the biochemical analysis (Fig. 5B). The data reveals that CT dimerization contributes to the stability of Cx45 at the junctional plaque.

### 4.5. CT dimerization is necessary for proper channel function

To determine whether inhibition of CT dimerization affects cell-to-cell communication (level and selectivity), junctional transfer of the tracer's neurobiotin (cationic) and Lucifer

Yellow(anionic) was measured in a scrape-loading assay using the stably transfected Cx45 WT and 6E MDCK cells. Texas Red Dextran (10,000 Da; junction impermeable) marks the loaded cells. Similar to previously published studies, Cx45 WT expressing cells were extensively coupled with respect to neurobiotin demonstrating greater than a fifth order dye transfer (i.e., cell layers past scrape) (Fig. 5C, top panels). In addition, Cx45 WT cells were impermeable to Lucifer Yellow [34]. Cx45 6E expressing cells were similar to WT with respect to being impermeable to Lucifer Yellow, however, coupling to neurobiotin was significantly reduced (second order dye transfer) (Fig. 5C, bottom panels). These results indicate that CT dimerization is important for proper Cx45 gap junction intercellular communication. The reduced junctional dye transfer could be explained by fewer junctional channels, reduced channel open time, or by reduced permeability to neurobiotin.

We next tested for altered hemichannel activity. Here we used $Ca^{2+}$ washout, a method known to activate connexin hemichannels, and measure the uptake of neurobiotin. In the control ($+Ca^{2+}$), both Cx45 WT and 6E expressing MDCK cells minimally took up the tracer (Fig. 6). However, after $Ca^{2+}$ washout, Cx45 6E expressing cells took up approximately 2 fold (DAPI normalized) more neurobiotin than the Cx45 WT cells. Importantly, WT expressing cells treated with 100 μM pervanadate (general inhibitor of protein tyrosine phosphatases) for 15 min to increase tyrosine phosphorylation did not alter dye uptake compared to untreated cells (Fig. 6 and Supplemental Fig. 2). Furthermore, pervanadate did not bypass the requirement for $Ca^{2+}$ depletion to activate Cx45 hemichannels. To confirm that dye uptake was the result of Cx45 hemichannels rather than other membrane channels, cells were pretreated with $La^{3+}$, an inhibitor of connexin hemichannel activity. When pretreated with $La^{3+}$, both Cx45 WT and 6E cells had significantly reduced dye uptake when compared to the $Ca^{2+}$ washout condition. The dye transfer experiments, together, indicate Cx45 6E hemichannels and channels are permeable to neurobiotin. The differences in neurobiotin transfer (hemichannels-higher, channels-lower) are consistent with the location of Cx45 (hemichannels vs. channels) observed in the Triton X-100 solubility and live imaging data (albeit a change in channel permeability could also contribute).

### 4.6. Cx45CT dimerization affects tyrosine phosphorylation, protein partner interactions, and hemichannel currents

To determine what regulatory mechanisms are influenced by CT dimerization, we examined for Cx45 WT and 6E three known characteristics of the CT domain: sites of phosphorylation, binding of protein partners, and modulation of channel properties. A consistent observation of cardiac connexins is altered gap junction intercellular communication caused by phosphorylation [29, 34–36]. Therefore, Cx45 WT and 6E were immunoprecipitated from the MDCK cells and Western blotted with a general anti-pY antibody (Fig. 7A) and anti-pS antibody (Supplemental. Fig. 3A). The data indicates a significant ~2-fold increase in tyrosine phosphorylation and no difference in serine phosphorylation of Cx45 6E compared with WT.

The decreased number of junctional channels, altered membrane localization, and increased amount of protein at the plasma membrane for the Cx45 6E suggests altered trafficking to,

at, and from the plasma membrane. Tyrosine phosphorylation affects connexin trafficking; our previous studies and those of others revealed that Src can inhibit Cx43 interactions with the cytoskeleton proteins β-tubulin, developmentally regulated brain protein (Drebrin), and Zonula Occludens 1 (ZO-1), leading to decreased gap junction intercellular communication [37–39]. To test if the increased tyrosine phosphorylation of Cx45 6E is affected in a similar manner, Cx45 WT and 6E were immunoprecipitated from MDCK cells and Western blotted for β-tubulin (Fig. 7B), Drebrin (Fig. 7C), and ZO-1 (Supplemental Fig. 3B). Comparing the amount immunoprecipitated between Cx45 6E and WT, observed were a significant ~3-fold decrease in β-tubulin, a significant ~2-fold increase in Drebrin, and no difference in ZO-1. These results suggest that one possible cause of the phenotype difference between WT and 6E is altered interactions the cytoskeleton.

Another possible cause of decreased 6E turnover is altered interactions with proteins involved in degradation. Studies have demonstrated that the neural precursor cell expressed developmentally down-regulated protein 4 (Nedd4), an E3 ubiquitin ligase, is a critical mediator of Cx43 gap junction turnover [40–42]. Additionally, the protein tumor susceptibility gene 101 (TSG101) mediates Cx43 trafficking to lysosomes [43]. Therefore, Cx45 WT and 6E were immunoprecipitated from MDCK cells and Western blotted for Nedd4 (Fig. 7D) and TSG101 (Supplemental Fig. 3C). The data indicates that relative to WT, the 6E shows a significant ~2-fold decrease in co-immunoprecipitated Nedd4 and no difference with TSG101.

Finally, the hemichannel currents of Cx45 WT and the 6E channels were assessed by electrophysiology. Xenopus oocytes were injected with the same amount of Cx45 WT or 6E cRNA, together with DNA antisense to the endogenous XenCx38. The oocytes were voltage-clamped and macroscopic currents of the hemichannels recorded during steps to depolarizing voltages to activate the channels [44, 45] (Fig. 8). The macroscopic currents elicited by depolarization were much greater for the 6E mutant than for the WT channels. The results illustrated are representative of data from multiple injected oocytes (WT, n=8; 6E, n=4). These records demonstrate that the 6E mutant is functional, and more important, that it mediates much greater hemichannel currents than WT under the same conditions. The increased currents due to 6E could be explained by any of several factors or a combination of them: greater plasma membrane expression of 6E hemichannels than for WT, dramatically shifted Po-V relations, or greater unitary conductance of the channels. The key point, however, is that the disruption of CT dimerization effected by the 6E mutation causes a dramatic increase in the magnitude of currents mediated by the channel compared to WT.

## 5. Discussion

Previously, we identified *in vitro* a structural feature unique to the Cx45 isoform, high affinity CT dimerization ($K_D$ ~100 nM). The Cx45CT dimerization domain (A333-N361) is highly conserved (72.4%) across species; five of the six-targeted hydrophobic residues are identical in all orthologs and the other highly conserved (Fig. 1). A BLAST search of Cx45CT residues A333-N361 within the human genome resulted in no significant homology to any other protein, indicating the uniqueness of this structure to Cx45. Based on the known effects of protein binding interactions of other connexin CTs (especially the Cx43CT), it

stands to reason that inhibiting this protein-protein interaction would influence the properties of Cx45. The specific inferred effects we observed from the absence of dimerization include: increased protein at the plasma membrane due to inhibited degradation, decreased plaque formation, increased hemichannel activity, retained regulation by $Ca^{+2}$, increased tyrosine phosphorylation, decreased interaction with β-tubulin and Nedd4, increased interaction with Drebrin, maintained interaction with ZO-1, and increased macroscopic currents.

Only a limited number of studies have characterized the functional role of the Cx45CT domain, largely in the context of co-expression with Cx43. For example, Cx45 WT (chicken) and CT truncated constructs (deletion of the last 34 and 37 residues) were transfected into a rat osteosarcoma cell line (ROS) that expresses endogenous Cx43 [46]. All proteins were transported to the plasma membrane with Cx45 WT and Δ34 displaying a punctate staining pattern, while the Cx45 Δ37 protein staining was more linear [47]. Neither of these truncations would have removed any of the key hydrophobic residues involved in CT dimerization. The difference lies in that the Cx45 Δ37 protein was more soluble in 1% Triton X-100 and did not co-precipitate with the actin-binding protein ZO-1 [47]. These observations are similar with the Cx45 6E in that alteration with the cytoskeleton (decreased binding of β-tubulin and increase binding of Drebrin) and proteins involved in connexin degradation (decreased binding of Nedd4) affects membrane localization and gap junction intercellular communication. Additional truncation studies suggest potential regulatory roles mediated by the Cx45 CT domain, however the relevance to dimerization cannot be clearly established at this time, these include regulating gap junctional conductance, channel permeability, and the ability of Cx45 to interact with Cx43 [46, 48–50]. Interestingly, expression of the Cx45CT domain, unlike the Cx40CT, failed to restore pH sensitivity to Cx43CT truncated channels [51]; when the Cx45CT was directly tethered to Cx43 or Cx40 (i.e., Cx43-Cx45CT or Cx40-Cx45CT), they did not form functional channels [50].

Many of the mechanisms involved in connexin regulation involve phosphorylation [52–55]. The negative charge of the phosphate could affect the permeability of ions to the pore, alter the structure of the transmembrane α-helices to influence pore size, or modify the binding affinities of protein partners involved in regulating connexins. Notably, if phosphorylation alters the kinetics of channel assembly or degradation (e.g., Nedd4; [40–42]), cell-to-cell communication will be altered. Only a few studies have addressed the role of phosphorylation in the regulation of Cx45. Phosphoamino acid analysis revealed phosphorylation of Cx45 serine, threonine, and tyrosine residues and deletion of the last 26 residues (contains 9 Ser) reduced phosphorylation [48]. In the case of regulation by Ser phosphorylation, little correlation exists between Cx43 and Cx45. Clear examples are activation of PKA by 8-Br-cAMP decreases Cx45 and increases Cx43 junctional conductance [35, 56], and activation of PKG by 8-Br-cGMP has no effect on Cx45, yet decreases Cx43 junctional conductance [35, 56]. In the case of the PKC activating phorbol ester PMA, Cx43 junctional conductance is decreased [34], however two studies show conflicting junctional conductance data for Cx45 (increase in [35] and decreased in [34]). Additionally, in the Martinez et al. [34] study, while Cx45 and Cx43 junctional conductance decreased, PMA only reduced transfer of the tracer neurobiotin in Cx43 expressing cells. In one further contrast to Cx43, Cx45 phosphorylation does not alter the single channel

conductance (22 and 42 pS), suggesting modification affects the open probability of Cx45 gap junction channels [35].

One example of commonality between Cx43 and Cx45 does occur in the regulation of junctional conductance by pervanadate. Promoting tyrosine phosphorylation of the CT domain reduces both Cx43 and Cx45 gap junction intercellular communication [35, 57, 58]; however, the mechanism(s) that achieve this may be different. For example, the majority of Cx43 in cells exposed to pervanadate are localized in the cytoplasm [59], while we observed that Cx45 is still localized at the plasma membrane. One explanation is that the only soluble tyrosine kinases identified to phosphorylate Cx43 (Src and Tyk2; residues Y247 and Y265) inhibit binding of β-tubulin and Drebrin, as well as Src also directly interacts with ZO-1 to inhibit Cx43/ZO-1 [37, 38]. Thus, affecting the interaction of Cx43 with microtubules and actin would explain the cytoplasmic localization of Cx43. However, although the tyrosine kinases were not identified, increased tyrosine phosphorylation of the Cx45 6E did not affect the Cx45 interaction with ZO-1 (actin), enhanced the interaction with Drebrin (actin), and a decreased interaction with β-tubulin (microtubules) and Nedd4. With ZO-1 regulating gap junction plaque size and assembly [60, 61], our data supports that β-tubulin is critical for plaque formation [62–64] and that Drebrin stabilizes connexins at the plasma membrane [38, 65]. These data would explain why pervanadate had no effect on Cx45 hemichannel activity in the presence or absence of $Ca^{+2}$.

Gap junctions in the ventricle are primarily composed of Cx43. In the failing heart, Cx43 remodeling contributes to the arrhythmic substrate. However, the failing heart also aberrantly upregulates Cx45 expression, normally expressed at very low levels, whose channel properties (low conductance, high voltage-sensitivity) greatly enhance propensity for serious arrhythmias [12–14]. The effect of Cx45 is disproportionate to the degree of upregulation, since it forms heteromeric channels with Cx43, and exerts a dominant-negative effect on the resulting gap junctions [20, 34, 49, 66]. Unfortunately, little is known about the determinants of the properties of Cx45 that make its expression in the myocardium so dangerous. Based upon the results provided herein, Cx45CT dimerization is a necessary structural feature for correct Cx45 function. Future studies need to pinpoint the regulatory role(s) mediated by Cx45CT dimerization, including if dimerization contributes to the dominant-negative phenotype in Cx43-Cx45 heteromeric channels, as well as define how kinases and protein partners that interact with the CT domain differentially regulate Cx43 and Cx45 function.

## Supplementary Material

Refer to Web version on PubMed Central for supplementary material.

## Acknowledgments

**Sources of Funding**

This work was supported by NIH Grants GM072631 to Paul Sorgen and GM103427 to Jim Turpen. Support for the UNMC Advanced Microscopy Core Facility was provided by the Nebraska Research Initiative, the Fred and Pamela Buffett Cancer Center Support Grant (P30CA036727), and an Institutional Development Award (IDeA)

from the NIGMS of the NIH (P30GM106397). The following NIH SIG funded instruments were used: LSM 710 Zeiss Confocal Microscope (NIH S10RR027301).

We thank Janice A. Taylor and James R. Talaska of the Advanced Microscopy Core Facility at the University of Nebraska Medical Center for providing assistance with confocal microscopy.

## References

1. Nielsen MS, Axelsen LN, Sorgen PL, Verma V, Delmar M, Holstein-Rathlou NH. Gap junctions. Comprehensive Physiology. 2012; 2(3):1981–2035. [PubMed: 23723031]
2. Palatinus JA, Rhett JM, Gourdie RG. The connexin43 carboxyl terminus and cardiac gap junction organization. Biochim Biophys Acta. 2012; 1818(8):1831–43. [PubMed: 21856279]
3. Moreno AP, Chanson M, Elenes S, Anumonwo J, Scerri I, Gu H, Taffet SM, Delmar M. Role of the carboxyl terminal of connexin43 in transjunctional fast voltage gating. Circ Res. 2002; 90(4):450–7. [PubMed: 11884375]
4. Morley GE, Taffet SM, Delmar M. Intramolecular interactions mediate pH regulation of connexin43 channels. Biophys J. 1996; 70(3):1294–302. [PubMed: 8785285]
5. Anumonwo JM, Taffet SM, Gu H, Chanson M, Moreno AP, Delmar M. The carboxyl terminal domain regulates the unitary conductance and voltage dependence of connexin40 gap junction channels. Circ Res. 2001; 88(7):666–73. [PubMed: 11304488]
6. Ghatnekar GS, Grek CL, Armstrong DG, Desai SC, Gourdie RG. The effect of a connexin43-based Peptide on the healing of chronic venous leg ulcers: a multicenter, randomized trial. J Invest Dermatol. 2015; 135(1):289–98. [PubMed: 25072595]
7. O'Quinn MP, Palatinus JA, Harris BS, Hewett KW, Gourdie RG. A peptide mimetic of the connexin43 carboxyl terminus reduces gap junction remodeling and induced arrhythmia following ventricular injury. Circ Res. 2011; 108(6):704–15. [PubMed: 21273554]
8. Verma V, Larsen BD, Coombs W, Lin X, Spagnol G, Sorgen PL, Taffet SM, Delmar M. Novel pharmacophores of connexin43 based on the "RXP" series of Cx43-binding peptides. Circ Res. 2009; 105(2):176–84. [PubMed: 19556520]
9. Rackauskas M, Neverauskas V, Skeberdis VA. Diversity and properties of connexin gap junction channels. Medicina (Kaunas). 2010; 46(1):1–12.
10. Desplantez T, Halliday D, Dupont E, Weingart R. Cardiac connexins Cx43 and Cx45: formation of diverse gap junction channels with diverse electrical properties. Pflugers Arch. 2004; 448(4):363–75. [PubMed: 15048573]
11. Severs NJ, Bruce AF, Dupont E, Rothery S. Remodelling of gap junctions and connexin expression in diseased myocardium. Cardiovasc Res. 2008; 80(1):9–19. [PubMed: 18519446]
12. Bao M, Kanter EM, Huang RY, Maxeiner S, Frank M, Zhang Y, Schuessler RB, Smith TW, Townsend RR, Rohrs HW, Berthoud VM, Willecke K, Laing JG, Yamada KA. Residual Cx45 and its relationship to Cx43 in murine ventricular myocardium. Channels (Austin). 2011; 5(6):489–99. [PubMed: 22127232]
13. Coppen SR, Severs NJ, Gourdie RG. Connexin45 (alpha 6) expression delineates an extended conduction system in the embryonic and mature rodent heart. Dev Genet. 1999; 24(1–2):82–90. [PubMed: 10079513]
14. Beauchamp P, Choby C, Desplantez T, de Peyer K, Green K, Yamada KA, Weingart R, Saffitz JE, Kleber AG. Electrical propagation in synthetic ventricular myocyte strands from germline connexin43 knockout mice. Circ Res. 2004; 95(2):170–8. [PubMed: 15192022]
15. Veeraraghavan R, Lin J, Hoeker GS, Keener JP, Gourdie RG, Poelzing S. Sodium channels in the Cx43 gap junction perinexus may constitute a cardiac ephapse: an experimental and modeling study. Pflugers Arch. 2015; 467(10):2093–105. [PubMed: 25578859]
16. Veeraraghavan R, Lin J, Keener JP, Gourdie R, Poelzing S. Potassium channels in the Cx43 gap junction perinexus modulate ephaptic coupling: an experimental and modeling study. Pflugers Arch. 2016; 468(10):1651–61. [PubMed: 27510622]
17. Betsuyaku T, Nnebe NS, Sundset R, Patibandla S, Krueger CM, Yamada KA. Overexpression of cardiac connexin45 increases susceptibility to ventricular tachyarrhythmias in vivo. Am J Physiol Heart Circ Physiol. 2006; 290(1):H163–71. [PubMed: 16126808]

18. van Rijen HV, Eckardt D, Degen J, Theis M, Ott T, Willecke K, Jongsma HJ, Opthof T, de Bakker JM. Slow conduction and enhanced anisotropy increase the propensity for ventricular tachyarrhythmias in adult mice with induced deletion of connexin43. Circulation. 2004; 109(8): 1048–55. [PubMed: 14967725]
19. Danik SB, Liu F, Zhang J, Suk HJ, Morley GE, Fishman GI, Gutstein DE. Modulation of cardiac gap junction expression and arrhythmic susceptibility. Circ Res. 2004; 95(10):1035–41. [PubMed: 15499029]
20. Yamada KA, Rogers JG, Sundset R, Steinberg TH, Saffitz J. Up-regulation of connexin45 in heart failure. J Cardiovasc Electrophysiol. 2003; 14(11):1205–12. [PubMed: 14678136]
21. Spragg DD, Leclercq C, Loghmani M, Faris OP, Tunin RS, DiSilvestre D, McVeigh ER, Tomaselli GF, Kass DA. Regional alterations in protein expression in the dyssynchronous failing heart. Circulation. 2003; 108(8):929–32. [PubMed: 12925451]
22. Kostin S, Rieger M, Dammer S, Hein S, Richter M, Klovekorn WP, Bauer EP, Schaper J. Gap junction remodeling and altered connexin43 expression in the failing human heart. Mol Cell Biochem. 2003; 242(1–2):135–44. [PubMed: 12619876]
23. Zhong G, Akoum N, Appadurai DA, Hayrapetyan V, Ahmed O, Martinez AD, Beyer EC, Moreno AP. Mono-Heteromeric Configurations of Gap Junction Channels Formed by Connexin43 and Connexin45 Reduce Unitary Conductance and Determine both Voltage Gating and Metabolic Flux Asymmetry. Frontiers in Physiology. 2017; 8(346)
24. Kopanic JL, Al-mugotir MH, Kieken F, Zach S, Trease AJ, Sorgen PL. Characterization of the connexin45 carboxyl-terminal domain structure and interactions with molecular partners. Biophys J. 2014; 106(10):2184–95. [PubMed: 24853747]
25. Kopanic JL, Sorgen PL. Chemical shift assignments of the connexin45 carboxyl terminal domain: monomer and dimer conformations. Biomol NMR Assign. 2013; 7(2):293–7. [PubMed: 23070843]
26. Bosanac I, Michikawa T, Mikoshiba K, Ikura M. Structural insights into the regulatory mechanism of IP3 receptor. Biochim Biophys Acta. 2004; 1742(1–3):89–102. [PubMed: 15590059]
27. Sievers F, Wilm A, Dineen D, Gibson TJ, Karplus K, Li W, Lopez R, McWilliam H, Remmert M, Soding J, Thompson JD, Higgins DG. Fast, scalable generation of high-quality protein multiple sequence alignments using Clustal Omega. Mol Syst Biol. 2011; 7:539. [PubMed: 21988835]
28. Mitra S, Annamalai L, Chakraborty S, Johnson K, Song XH, Batra SK, Mehta PP. Androgen-regulated formation and degradation of gap junctions in androgen-responsive human prostate cancer cells. Mol Biol Cell. 2006; 17(12):5400–16. [PubMed: 17050739]
29. Li H, Spagnol G, Naslavsky N, Caplan S, Sorgen PL. TC-PTP directly interacts with connexin43 to regulate gap junction intercellular communication. J Cell Sci. 2014; 127(Pt 15):3269–79. [PubMed: 24849651]
30. Puhar A, Tronchere H, Payrastre B, Nhieu GT, Sansonetti PJ. A Shigella effector dampens inflammation by regulating epithelial release of danger signal ATP through production of the lipid mediator PtdIns5P. Immunity. 2013; 39(6):1121–31. [PubMed: 24332032]
31. Stauch K, Kieken F, Sorgen P. Characterization of the structure and intermolecular interactions between the connexin 32 carboxyl-terminal domain and the protein partners synapse-associated protein 97 and calmodulin. J Biol Chem. 2012; 287(33):27771–88. [PubMed: 22718765]
32. Guan Y, Zhu Q, Huang D, Zhao S, Jan Lo L, Peng J. An equation to estimate the difference between theoretically predicted and SDS PAGE-displayed molecular weights for an acidic peptide. Sci Rep. 2015; 5:13370. [PubMed: 26311515]
33. Kausalya PJ, Reichert M, Hunziker W. Connexin45 directly binds to ZO-1 and localizes to the tight junction region in epithelial MDCK cells. FEBS Lett. 2001; 505(1):92–6. [PubMed: 11557048]
34. Martinez AD, Hayrapetyan V, Moreno AP, Beyer EC. Connexin43 and connexin45 form heteromeric gap junction channels in which individual components determine permeability and regulation. Circ Res. 2002; 90(10):1100–7. [PubMed: 12039800]
35. van Veen TA, van Rijen HV, Jongsma HJ. Electrical conductance of mouse connexin45 gap junction channels is modulated by phosphorylation. Cardiovasc Res. 2000; 46(3):496–510. [PubMed: 10912460]

36. Laing JG, Westphale EM, Engelmann GL, Beyer EC. Characterization of the gap junction protein, connexin45. J Membr Biol. 1994; 139(1):31–40. [PubMed: 8071985]
37. Saidi Brikci-Nigassa A, Clement MJ, Ha-Duong T, Adjadj E, Ziani L, Pastre D, Curmi PA, Savarin P. Phosphorylation controls the interaction of the connexin43 C-terminal domain with tubulin and microtubules. Biochemistry. 2012; 51(21):4331–42. [PubMed: 22558917]
38. Ambrosi C, Ren C, Spagnol G, Cavin G, Cone A, Grintsevich EE, Sosinsky GE, Sorgen PL. Connexin43 Forms Supramolecular Complexes through Non-Overlapping Binding Sites for Drebrin, Tubulin, and ZO-1. PLoS One. 2016; 11(6):e0157073. [PubMed: 27280719]
39. Sorgen PL, Duffy HS, Sahoo P, Coombs W, Delmar M, Spray DC. Structural changes in the carboxyl terminus of the gap junction protein connexin43 indicates signaling between binding domains for c-Src and zonula occludens-1. J Biol Chem. 2004; 279(52):54695–701. [PubMed: 15492000]
40. Spagnol G, Kieken F, Kopanic JL, Li H, Zach S, Stauch KL, Grosely R, Sorgen PL. Structural Studies of the Nedd4 WW Domains and their Selectivity for the Cx43 Carboxyl-terminus. J Biol Chem. 2016
41. Girao H, Catarino S, Pereira P. Eps15 interacts with ubiquitinated Cx43 and mediates its internalization. Exp Cell Res. 2009; 315(20):3587–97. [PubMed: 19835873]
42. Leykauf K, Salek M, Bomke J, Frech M, Lehmann WD, Durst M, Alonso A. Ubiquitin protein ligase Nedd4 binds to connexin43 by a phosphorylation-modulated process. J Cell Sci. 2006; 119(Pt 17):3634–42. [PubMed: 16931598]
43. Leithe E, Kjenseth A, Sirnes S, Stenmark H, Brech A, Rivedal E. Ubiquitylation of the gap junction protein connexin-43 signals its trafficking from early endosomes to lysosomes in a process mediated by Hrs and Tsg101. J Cell Sci. 2009; 122(Pt 21):3883–93. [PubMed: 19808888]
44. Lopez W, Liu Y, Harris AL, Contreras JE. Divalent regulation and intersubunit interactions of human connexin26 (Cx26) hemichannels. Channels (Austin). 2014; 8(1):1–4. [PubMed: 24126106]
45. Lopez W, Gonzalez J, Liu Y, Harris AL, Contreras JE. Insights on the mechanisms of Ca2+ regulation of connexin26 hemichannels revealed by human pathogenic mutations (D50N/Y). J Gen Physiol. 2013; 142(1):23–35. [PubMed: 23797420]
46. Koval M, Geist ST, Westphale EM, Kemendy AE, Civitelli R, Beyer EC, Steinberg TH. Transfected connexin45 alters gap junction permeability in cells expressing endogenous connexin43. J Cell Biol. 1995; 130(4):987–95. [PubMed: 7642714]
47. Laing JG, Koval M, Steinberg TH. Association with ZO-1 correlates with plasma membrane partitioning in truncated connexin45 mutants. J Membr Biol. 2005; 207(1):45–53. [PubMed: 16463142]
48. Hertlein B, Butterweck A, Haubrich S, Willecke K, Traub O. Phosphorylated carboxy terminal serine residues stabilize the mouse gap junction protein connexin45 against degradation. J Membr Biol. 1998; 162(3):247–57. [PubMed: 9543497]
49. Hulser DF, Rutz ML, Eckert R, Traub O. Functional rescue of defective mutant connexons by pairing with wild-type connexons. Pflugers Arch. 2001; 441(4):521–8. [PubMed: 11212216]
50. Sahu G, Bera AK. Contribution of intracellular calcium and pH in ischemic uncoupling of cardiac gap junction channels formed of connexins 43, 40, and 45: a critical function of C-terminal domain. PLoS One. 2013; 8(3):e60506. [PubMed: 23536911]
51. Stergiopoulos K, Alvarado JL, Mastroianni M, Ek-Vitorin JF, Taffet SM, Delmar M. Hetero-domain interactions as a mechanism for the regulation of connexin channels. Circ Res. 1999; 84(10):1144–55. [PubMed: 10347089]
52. Axelsen LN, Calloe K, Holstein-Rathlou NH, Nielsen MS. Managing the complexity of communication: regulation of gap junctions by post-translational modification. Frontiers in pharmacology. 2013; 4:130. [PubMed: 24155720]
53. Solan JL, Lampe PD. Connexin phosphorylation as a regulatory event linked to gap junction channel assembly. Biochim Biophys Acta. 2005; 1711(2):154–63. [PubMed: 15955300]
54. Lampe PD, Lau AF. The effects of connexin phosphorylation on gap junctional communication. Int J Biochem Cell Biol. 2004; 36(7):1171–86. [PubMed: 15109565]

55. Solan JL, Lampe PD. Specific Cx43 phosphorylation events regulate gap junction turnover in vivo. FEBS Lett. 2014; 588(8):1423–9. [PubMed: 24508467]
56. Burt JM, Spray DC. Inotropic agents modulate gap junctional conductance between cardiac myocytes. Am J Physiol. 1988; 254(6 Pt 2):H1206–10. [PubMed: 2837915]
57. Mikalsen SO, Husoy T, Vikhamar G, Sanner T. Induction of phosphotyrosine in the gap junction protein, connexin43. FEBS Lett. 1997; 401(2–3):271–5. [PubMed: 9013902]
58. Giepmans BN, Feiken E, Gebbink MF, Moolenaar WH. Association of connexin43 with a receptor protein tyrosine phosphatase. Cell Commun Adhes. 2003; 10(4–6):201–5. [PubMed: 14681016]
59. Cruciani V, Mikalsen SO. Stimulated phosphorylation of intracellular connexin43. Exp Cell Res. 1999; 251(2):285–98. [PubMed: 10471314]
60. Laing JG, Chou BC, Steinberg TH. ZO-1 alters the plasma membrane localization and function of Cx43 in osteoblastic cells. J Cell Sci. 2005; 118(Pt 10):2167–76. [PubMed: 15855237]
61. Rhett JM, Jourdan J, Gourdie RG. Connexin 43 connexon to gap junction transition is regulated by zonula occludens-1. Mol Biol Cell. 2011; 22(9):1516–28. [PubMed: 21411628]
62. Guo Y, Martinez-Williams C, Rannels DE. Gap junction-microtubule associations in rat alveolar epithelial cells. Am J Physiol Lung Cell Mol Physiol. 2003; 285(6):L1213–21. [PubMed: 14604851]
63. Shaw RM, Fay AJ, Puthenveedu MA, von Zastrow M, Jan YN, Jan LY. Microtubule plus-end-tracking proteins target gap junctions directly from the cell interior to adherens junctions. Cell. 2007; 128(3):547–60. [PubMed: 17289573]
64. Wang D, Xing W, Wang X, Zhu H. Taxol stabilizes gap junctions and reduces ischemic ventricular arrhythmias in rats in vivo. Molecular medicine reports. 2015; 11(5):3243–8. [PubMed: 25544595]
65. Butkevich E, Hulsmann S, Wenzel D, Shirao T, Duden R, Majoul I. Drebrin is a novel connexin-43 binding partner that links gap junctions to the submembrane cytoskeleton. Curr Biol. 2004; 14(8): 650–8. [PubMed: 15084279]
66. Moreno AP, Laing JG, Beyer EC, Spray DC. Properties of gap junction channels formed of connexin 45 endogenously expressed in human hepatoma (SKHep1) cells. Am J Physiol. 1995; 268(2 Pt 1):C356–65. [PubMed: 7532358]

## Highlights

- Identified high affinity dimerization ($K_D$ ~100 nM) of Cx45CT domains
- CT dimerization is required for proper Cx45 localization and phosphorylation status
- Cx45CT dimerization mediates normal cell-cell coupling and hemichannel activity
- CT dimerization is a structural feature important for correct Cx45 function

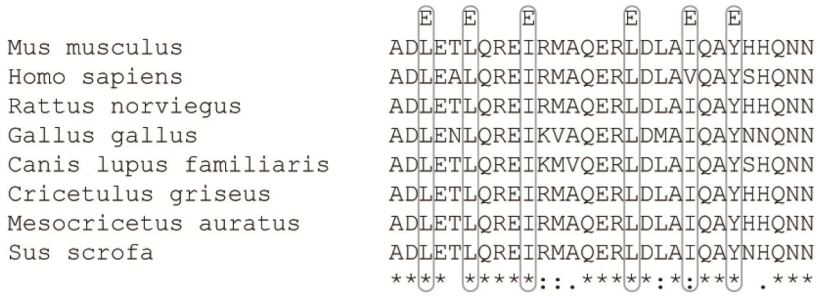


**Figure 1. Sequence alignment of the Cx45CT dimerization domain (A333-N361) from different species**

Sequence alignment of the A333-N361 region using Clustal Omega to all available Cx45 RefSeq sequences revealed a high degree of conservation within this region, with 72.4% identical, 20.6% conserved, and 6.9% non-conserved residues. For clarity, the sites of point mutations in the Cx45 6E construct are indicated by the single letter code above the alignments. Degree of site conservation (excluding Cx45 6E mutations) is indicated at the bottom, * = identical, : and . = high conservation and intermediate conservation, respectively.

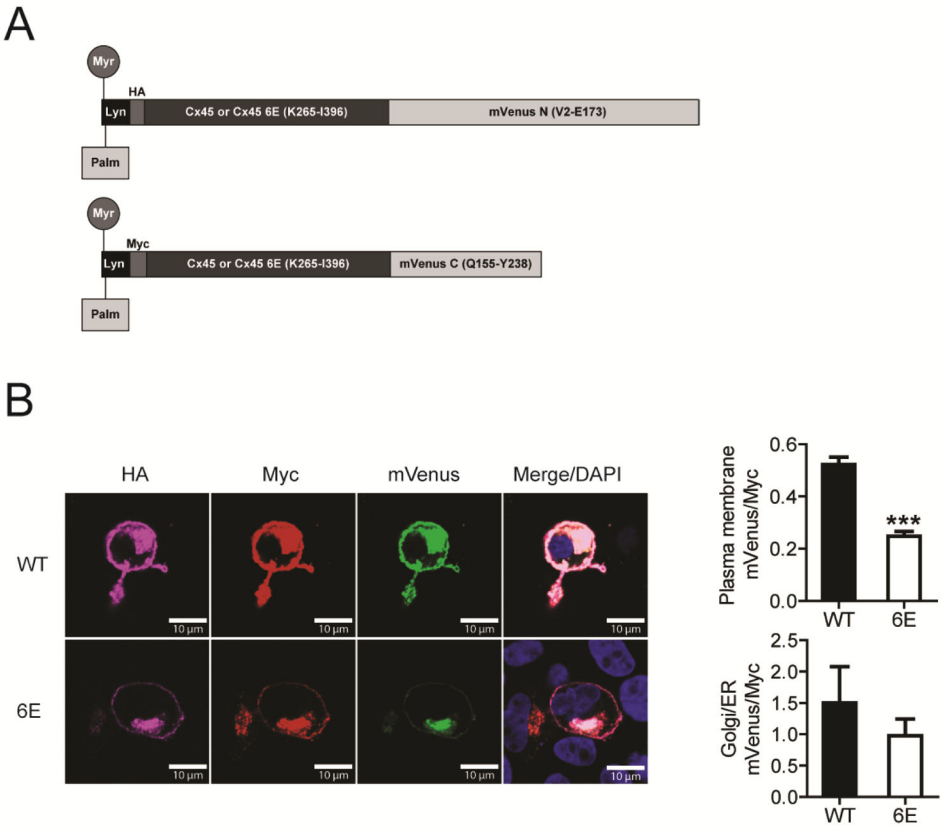


**Figure 2. Cx45CT dimerization at the plasma membrane**

MDCK cells transiently transfected with the Cx45CT WT or 6E versions of Lyn-HA-CxCT-mVenN and Lyn-Myc-CxCT-mVenC were assessed for complemented mVenus signal. A) Schematic of the protein constructs with post-translational modifications resulting in the addition of the myristoyl and palmitoyl groups. B) Representative immunofluorescence images of double transfected MDCK cells. Calculated area under the curve and mean fluorescent intensity of mVenus signal normalized to Myc tag fluorescence at the plasma membrane (top) and Golgi/ER (bottom), respectively. Statistics are one tailed unpaired student's T-test between the Cx45CT WT and 6E groups; ***$P$>0.0001. Scale bar = 10 µm.

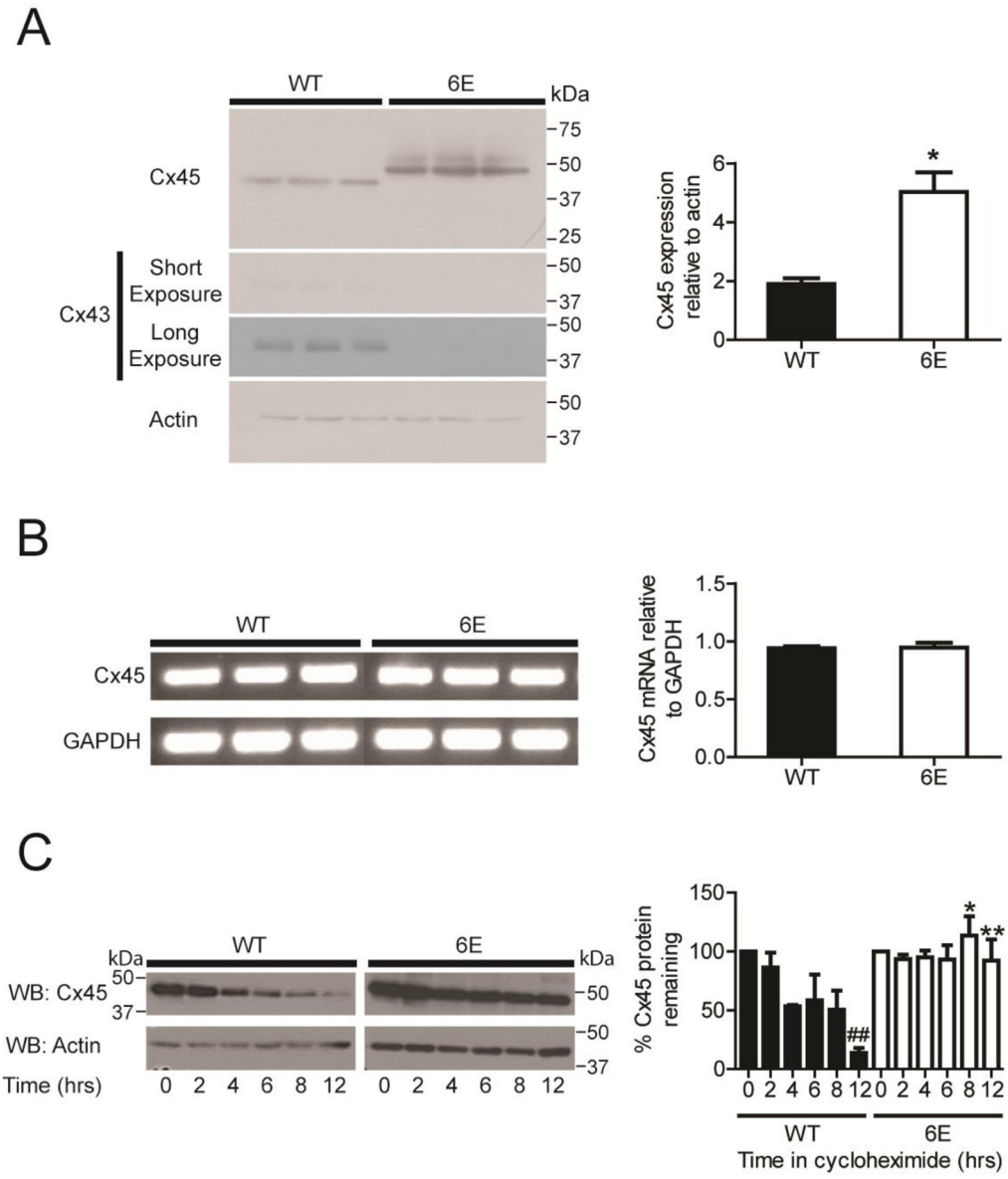


**Figure 3. Inhibiting Cx45CT dimerization decreases protein degradation**

Three different MDCK cells expressing either Cx45 WT or 6E were assessed for expression at the protein and transcript levels. A) Western blots and quantification of Cx45 WT, Cx45 6E, and Cx43 expression. B) RT-PCR gel images and quantification of Cx45 WT and 6E transcripts. C) Western blots and quantification of Cx45 WT or 6E subjected to a 12 hr cycloheximide chase. Results presented as the mean + s.e.m. (n=3). Statistics are used to analyze the data were two-tailed unpaired Student's T-test (A, n=3, $*P<0.05$; and C, n=3, n.s., $*P<0.9056$) and one-way ANOVA with a Neuman-Keuls post hoc test (B, n=3; $*P<0.05$, $**P<0.001$ comparing Cx45 WT and 6E, and $^{\#\#}P<0.001$ compared to time = 0).

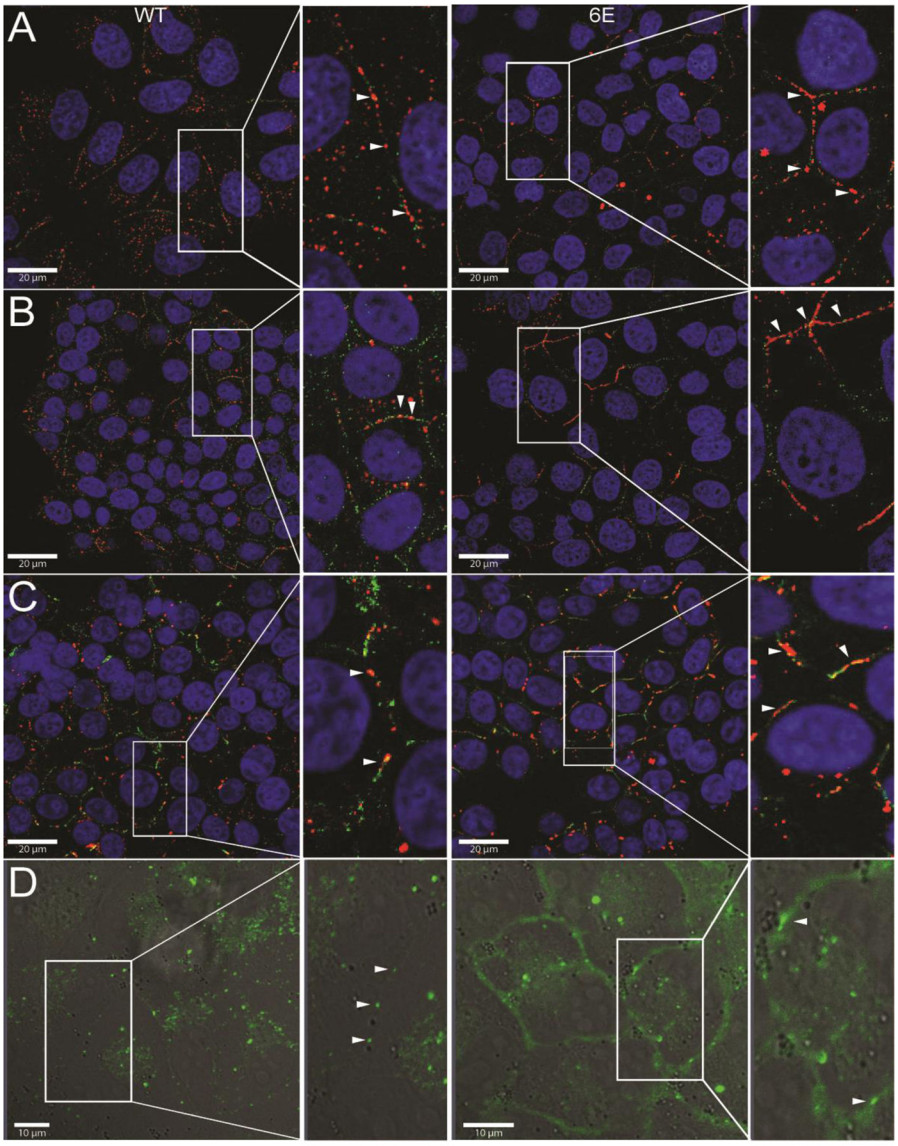


**Figure 4. Inhibiting Cx45CT dimerization alters Cx45 cellular localization**

Representative immunofluorescence images (red) of methanol fixed cells stably expressing Cx45 WT (left) or 6E (right). Co-immunostaining (green) for either E-Cadherin (MDCK) or β-catenin (Hek-293T) was used to mark the plasma membranes of the fixed cells (blue = DAPI). A) Clonally selected MDCK cells stably expressing mouse Cx45 WT or 6E. B) Bulk selected MDCK cells stably expressing human Cx45 WT or 6E. C) Bulk selected Hek-293T cells stably expressing mouse Cx45 WT and 6E. D) Isolated time-lapse frames of clonally selected MDCK cells expressing C-terminal eGFP fusions of mouse Cx45 WT or 6E (green). White arrows in the insets indicate gap junction plaques. Scale bar A–C = 20 μm and D = 10 μm.

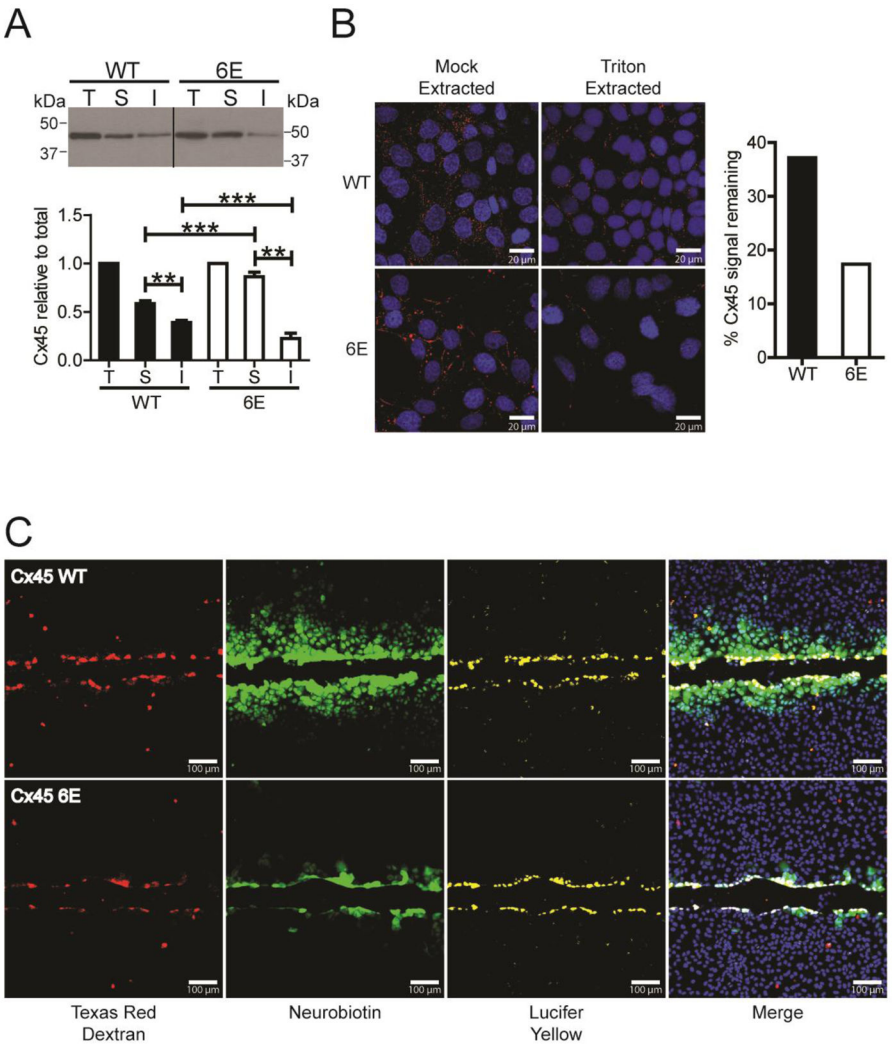


**Figure 5. Inhibiting Cx45CT dimerization impairs gap junction intercellular communication**

Triton X-100 solubility was used to compare MDCK cells expressing Cx45 WT or 6E. A) Western blot image of Triton X-100 extracted protein; total lysate (T), soluble (S), and insoluble (I) fractions. Below is the quantification of protein in the T, S, and I fractions. Statistics represent one-way ANOVA with a Neuman-Keuls post-hoc correction (n=3, $^{**}P<0.001$,$^{***}P<0.0001$). B) Representative fluorescent images (left) and quantification (right) of *in situ* Triton X-100 and mock (1x PBS) extracted Cx45 WT or 6E in MDCK cells (red, Cx45; blue, DAPI). C) MDCK cells expressing Cx45 WT (top) or 6E (bottom) were scrape loaded with tracer dyes to assess the degree of intercellular communication. Red, Texas red dextran (MW 10,000 Da); yellow, Lucifer yellow CH (MW 443 Da; −2 charge), green, neurobiotin (MW 287 Da; +1 charge); and blue, DAPI. Images are representative of greater than six independent experiments. Scale bar in B = 20 µm and C = 100 µm.

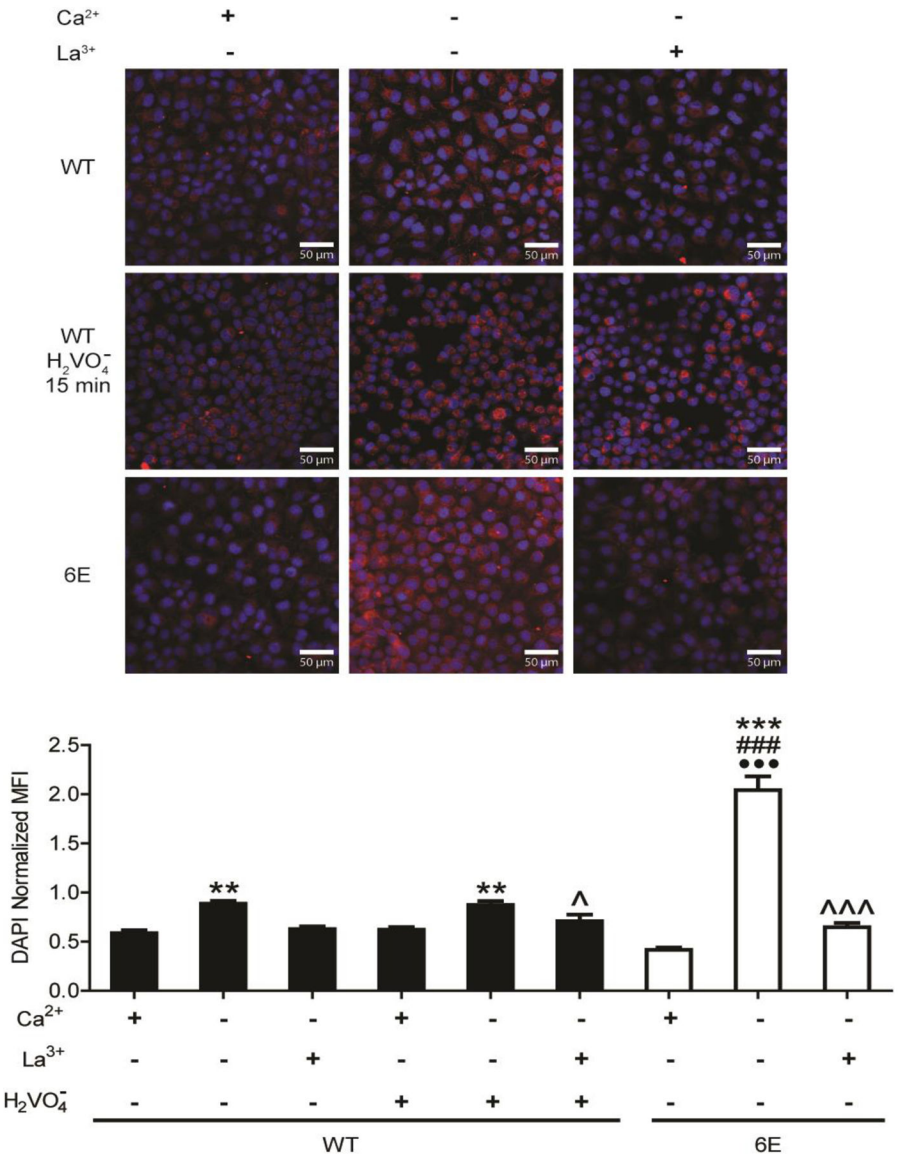


**Figure 6. Inhibiting Cx45CT dimerization affects hemichannel dye uptake**

MDCK cells stably expressing Cx45 WT or 6E were subjected to conditions that activate hemichannels activity ($Ca^{2+}$ deprivation) and the level of neurobiotin uptake was measured. Representative fluorescent micrographs of cells loaded with neurobiotin and probed with streptavidin-647 conjugate (red). Quantification of DAPI (blue) normalized mean fluorescent intensity (MFI) from 3 replicates, 15 random 100X FOVs were acquired per replicate. Statistics are one-way ANOVA with a Neuman-Keuls multiple comparison test (***$P$<0.0001 relative to +$Ca^{2+}$ within same group, ^ and ^^^$P$ <0.05 and <0.0001 respectively, relative to −$Ca^{2+}$ within same group; ###$P$<0.0001 between −$Ca^{2+}$ treatment groups; •••$P$<0.0001 compared to WT + pervanadate). Scale bar = 50 µm.

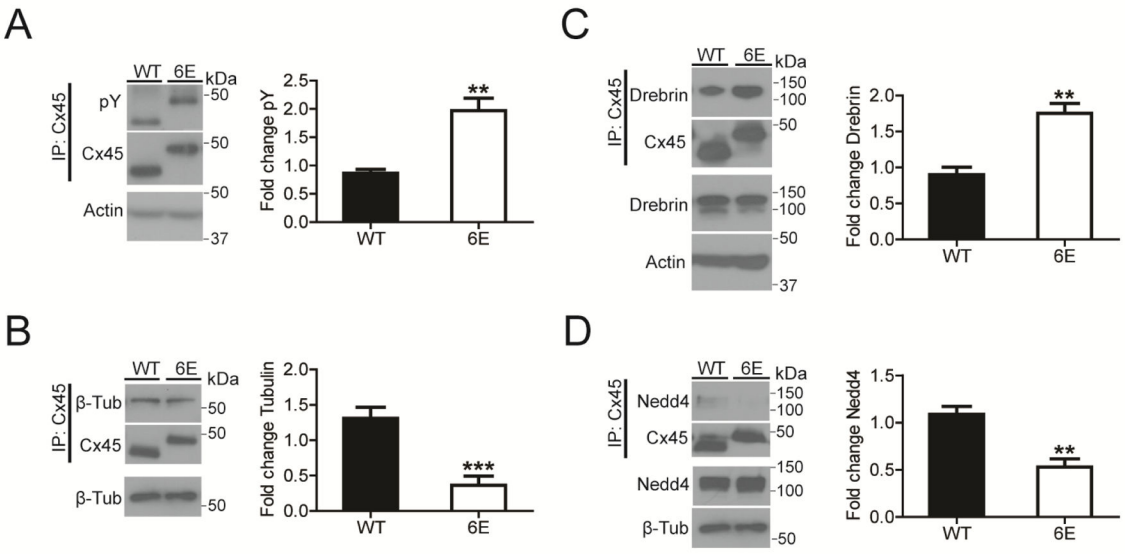


**Figure 7. Inhibiting Cx45CT dimerization alters phosphorylation and protein partner interactions**

MDCK cells stably expressing Cx45 WT or 6E were cultured, lysed, and immunoprecipitated to assess total phosphorylation levels and interactions with β-tubulin, Drebrin, and Nedd4. A) Representative Western blots of immunoprecipitated Cx45 WT or 6E blotting with a general anti-pY antibody. (n=3, ** $P<0.01$) Representative Western blot of B) β-tubulin (n=7, *** $P<0.001$), C) Drebrin (n=3, ** $P<0.01$), and D) Nedd4 (n=3, ** $P<0.01$) co-immunoprecipitated with either Cx45 WT or 6E. Data presented as mean fold change + s.e.m. relative to the first WT replicate. Statistics are two-tailed unpaired Student's T-test.

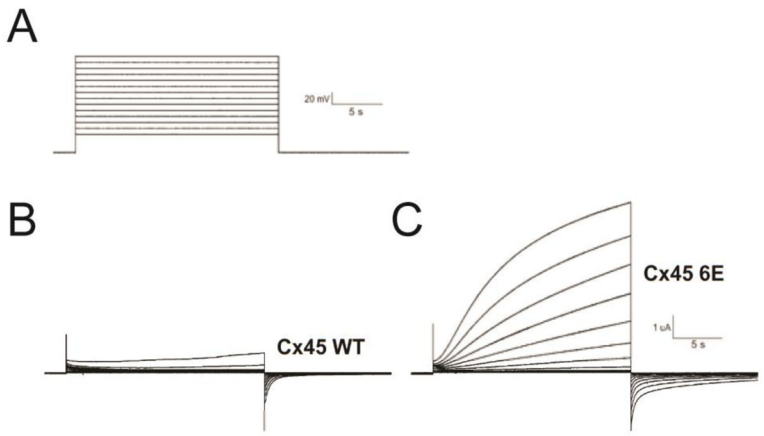


**Figure 8. Inhibiting Cx45CT dimerization affects hemichannel currents**

Oocytes injected with equal amounts of cRNA coding for Cx45 WT or the 6E mutant were voltage clamped and hemichannel currents elicited by large depolarizing voltage steps from −50 to +80 mV in 10 mV incrememts from a holding potential of −80 mV. A) Representation of voltage protocol. Under the same voltage protocols, the WT channels mediated substantially less current than the 6E channels. Representative current plots from (B) WT and (C) 6E expressing oocytes.